

Article

Spatiotemporal Evolution and Relationship between Night Time Light and Land Surface Temperature: A Case Study of Beijing, China

Zhe Li ¹, Feng Wu ², Huiqiang Ma ³, Zhanjun Xu ^{1,*} and Shaohua Wang ⁴

¹ College of Resources and Environment, Shanxi Agricultural University, Taigu 030801, China; s20212276@stu.sxau.edu.cn

² Key Laboratory of Land Surface Pattern and Simulation, Institute of Geographic Sciences and Natural Resources Research, Chinese Academy of Sciences, No. 11, Datun Road, Chaoyang District, Beijing 100101, China; wufeng@igsnr.ac.cn

³ Institute of Culture and Tourism, Shanxi University of Finance and Economic, Taiyuan 030012, China; mahuiqiang001@126.com

⁴ Key Laboratory of Digital Earth Science, Aerospace Information Research Institute, Chinese Academy of Sciences, Beijing 100094, China; wangshaohua@aircas.ac.cn

* Correspondence: zjxu163@126.com



Citation: Li, Z.; Wu, F.; Ma, H.; Xu, Z.; Wang, S. Spatiotemporal Evolution and Relationship between Night Time Light and Land Surface Temperature: A Case Study of Beijing, China. *Land* **2022**, *11*, 548. <https://doi.org/10.3390/land11040548>

Academic Editors: Baojie He, Ayyoob Sharifi, Chi Feng and Jun Yang

Received: 27 February 2022

Accepted: 5 April 2022

Published: 8 April 2022

Publisher's Note: MDPI stays neutral with regard to jurisdictional claims in published maps and institutional affiliations.



Copyright: © 2022 by the authors. Licensee MDPI, Basel, Switzerland. This article is an open access article distributed under the terms and conditions of the Creative Commons Attribution (CC BY) license (<https://creativecommons.org/licenses/by/4.0/>).

Abstract: Rapid urbanization has triggered significant changes in urban land surface temperature (LST), which in turn affects urban ecosystems and the health of residents. Therefore, exploring the interrelationship between urban development and LST can help optimize the urban thermal environment and promote sustainable development. Based on remote sensing data from 2004–2019 within the sixth ring road of Beijing, this study investigates the spatiotemporal coupling law of night time light (NTL) and LST using an overall coupling model and analyzes the degree of coordination between them using a coordination model. The spatial response law between them was also analyzed using standard deviation ellipses and bivariate spatial autocorrelation. The results show that, from the perspective of spatiotemporal evolution, the spatial distributions of NTL and LST within the sixth ring road of Beijing were closely related from 2004 to 2019, although the overall coupling of NTL and LST was initially decreased and then continuously increased. From the perspective of coordination types, the main types of coordination between NTL and LST deteriorated over time. The increase in LST lagged behind NTL from 2004 to 2009 (heating hysteresis type), while LST increased ahead of NTL from 2014 to 2019 (heating advance type). This suggests that urban development became less efficient, while LST increases became more significant. In terms of correlation, NTL and LST showed significant positive correlation and spatial positive correlation; the correlation coefficient first decreased significantly and then continued to increase. From 2004 to 2009, the temperature increase caused by urbanization was suppressed due to the 2008 Beijing Olympics and related ecological protection policies, resulting in a significant decrease in the correlation coefficient between NTL and LST. From 2009 to 2019, short-term measures taken by Beijing during the Olympic Games were no longer effective, and the opposition between urban development and related policies made the policies increasingly less effective, thereby increasing the correlation coefficient between NTL and LST, and the increase in LST was more significant. This will greatly affect the urban ecological environment and residents' health and make the previous government investment to suppress the temperature increase all in vain. This study can provide theoretical and practical support for the development of thermal environment optimization schemes and LST mitigation strategies in Beijing and other cities.

Keywords: urban development; night time light; land surface temperature; coordination model; spatial autocorrelation; Beijing

1. Introduction

Land surface temperature (LST), combining the results of all surface–atmosphere interactions and energy fluxes between the atmosphere and the ground, plays an important role in studying the urban thermal environment [1]. Since the implementation of The Reform and Opening-up Policy, China’s accelerated urbanization in recent decades has led to an increase in the LST in its urban areas, which directly affects urban air quality [2,3], the local climate [4–6], energy utilization [7], thermal comfort [8,9], and the biological community [10]. Furthermore, a high temperature environment can pose a threat to human health from both physiological and psychological aspects. It not only directly causes heat stroke and dehydration but also affects sleep quality and induces irritability and mental disorders, thus increasing the probability of depression and other psychological disorders [11–13]. These effects degrade the quality of the urban environment, which in turn slows down urban development. Therefore, exploring the relationship between urban development and LST can help guide the sustainable development of cities [14].

Most previous studies on the spatial distribution characteristics of LST and the influence of urban development on LST [15–23] mainly focused on two aspects [24]: (1) the characterization of the urban development using land cover factors, including land use-cover change [25–27], the normalized difference vegetation index (NDVI) [28–30] and normalized difference built-up index [31,32], impervious surface area, and impervious surface distribution density [33,34]; and (2) the characterization of the urban development using socioeconomic factors, including gross domestic product (GDP) [35], population density [36,37], and industrial production activities [38]. Furthermore, many studies have emphasized the importance of landscape composition and configuration in mitigating urban surface temperature elevation [16,39–41].

However, it is difficult to synthesize spatial urban development data using a single geographic element. Previous findings suggest that the indicators used to quantify urban development should cover three aspects: economy, population, and land [42]. In the past two decades, night time light (NTL) images have been rapidly developed. Compared with ordinary remote sensing satellite images, NTL images record surface light intensity information that more directly reflects intensity of human activities and are therefore widely used in urban studies, including for mapping urban areas [43] and detecting trends in urban spatial spread [44]; in addition, NTL imagery is considered a major data source for estimating changes in urban population size and density [45], detecting socioeconomic activities [46], measuring energy and electricity consumption [47], and assessing gas emissions [48]. The results of various studies show that the pixel values of NTL data are significantly correlated with various indicators for assessing urban development, such as economic density [49], population density [50], urbanization level [51], and energy consumption [52]. Most previous studies in this area have focused on the influence of urban development on LST; fewer studies have systematically analyzed the relationship between NTL and LST.

Methods such as Pearson’s correlation coefficient [53], linear regression analysis [36,54], and stepwise multiple linear regression [55] have been widely used to study the influence of various types of factors on LST. However, the above methods ignore the spatial heterogeneity of such factors and LST, resulting in an inability to adequately measure their interrelationships. In contrast, the overall coupling model can be used to analyze the level of coordination among variables [56,57], while the coordination model can capture the degree of coordination in the evolution of two variables [58]. These two methods are thus more appropriate to reveal the spatiotemporal coupling laws of NTL and LST than the aforementioned methods. In addition, the standard deviation ellipse can reflect the degree of concentration and dominant direction of the spatial pattern of variables [59], while bivariate spatial autocorrelation can effectively reflect the association and dependence characteristics of the spatial distribution of two types of variables [60]. These two techniques can be used to explore the spatial response law between NTL and LST.

Beijing is one of the most populous metropolitan areas in the world. Intensive human activities and urban development within the sixth ring road of Beijing have led to a

significant increase in the LST in this area, posing a major threat to human comfort and environmental health [61]. Therefore, based on remote sensing data obtained within the sixth ring road of Beijing from 2004 to 2019, the spatiotemporal coupling and correlation of NTL and the LST were explored in this study using an overall coupling model, a coordination model, standard deviation ellipse (SDE), and bivariate spatial autocorrelation. This study provides theoretical and practical support for the development of thermal environment optimization schemes and LST mitigation strategies in Beijing and other cities.

2. Materials and Methods

2.1. Study Area

As the capital of China, Beijing is located in the northern part of the North China ($39^{\circ}56' N$, $116^{\circ}20' E$). Its topography is high in the northwest and low in the southeast, and the total administrative area is $16,410 \text{ km}^2$ (Figure 1). The research area was defined as the area within the sixth ring road of Beijing, as this is where the city's population and diverse functions are concentrated. Therefore, it is a key area of urban construction in Beijing. From 2004 to 2019, the population of Beijing grew from 1492.7 million to 2190.1 million, with an increase of 697.4 million. GDP grew from 625.25 billion to 3544.51 billion, with an increase of 2919.26 billion. Population growth, economic development, and the hosting of large events such as the 2008 Olympic Games, among other factors, have led to accelerated urbanization within this area. From 2004 to 2019, the construction land in Beijing grew from 1708.61 km^2 to 2153.88 km^2 , with an increase of 445.27 km^2 . This means the conversion of considerable areas of natural surfaces into asphalt, cement, and other artificial surfaces, thus causing changes in LST and triggering a series of environmental problems such as the creation of urban heat islands [62].

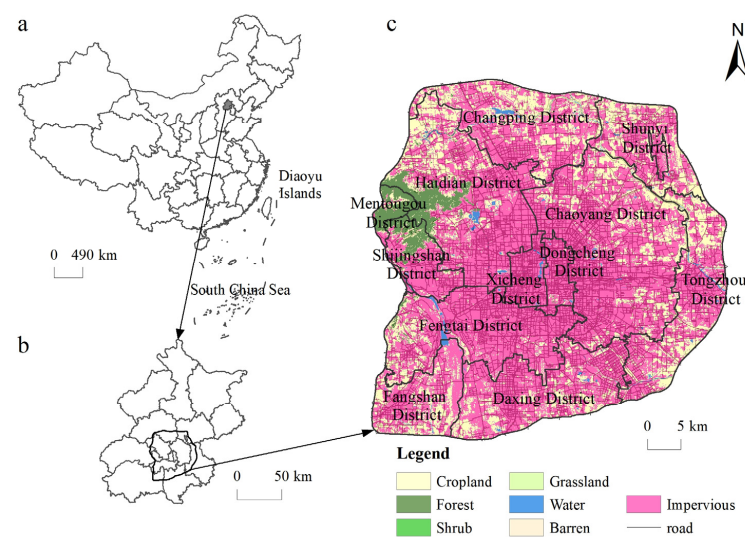


Figure 1. The geographical location of the study area: (a) China, (b) Beijing, (c) The sixth ring road of Beijing.

2.2. Data Sources

In this study, Landsat 5 TM and Landsat 8 OLI multispectral and thermal infrared remote sensing images were obtained from the United States Geological Survey (USGS) data center (<https://glovis.usgs.gov/>, accessed on 3 October 2021). Collection of remote sensing image data was conducted during the summer with clear weather, with a cloud cover of less than 10%. The remote sensing image is preprocessed by ENVI 5.3 software, such as radiometric calibration, atmospheric correction, and area of interest clipping [63]. Then, the images were classified into seven land cover categories, namely, cropland, forest, shrub, grassland, water, impervious land, and barren land. In this study, the NTL data used are Defense Meteorological Satellite Program/Operational Linescan System (DMSP/OLS) NTL data and National Polar-orbiting Operational Environmental Satellite System Preparatory Project/Visible Infrared Imaging Radiometer

Suite (NPP/VIIRS) NTL data (Table 1). The NTL data are preprocessed by ENVI 5.3 software, such as data fusion denoising, clipping, and radiometric correction [64]. Both NTL datasets were obtained from the National Geophysical Data Center website (<http://www.ngdc.noaa.gov/>, accessed on 3 October 2021).

Table 1. Data sources and descriptions.

Data	Data Identification	Time	Data Source
Landsat4-5 TM	LT51230322004252BJC00	8 September 2004	http://www.gscloud.cn/ , (accessed on 3 October 2021).
Landsat4-5 TM	LT51230322009265IKR00	22 September 2009	
Landsat8 OLI_TIRS	LC81230322014247LGN01	4 September 2014	
Landsat8 OLI_TIRS	LC81230322019261LGN00	18 September 2019	
DEM	ASTGTM_N39E116	-	
Road network	-	2020	https://www.openstreetmap.org/ , (accessed on 3 October 2021).
POI	-	2020	https://map.baidu.com/ , (accessed on 3 October 2021).
DMSF/OLS NTL	-	-	http://www.ngdc.noaa.gov/ , (accessed on 3 October 2021).
NPP/VIIRS NTL	-	-	

2.3. Methods

This study is based on remote sensing data obtained within the sixth ring road of Beijing from 2004 to 2019. The spatiotemporal coupling and correlation of NTL and LST were explored using an overall coupling model, a coordination model, and standard deviation ellipse (SDE). A flowchart depicting the methodology employed in this study is provided in Figure 2.

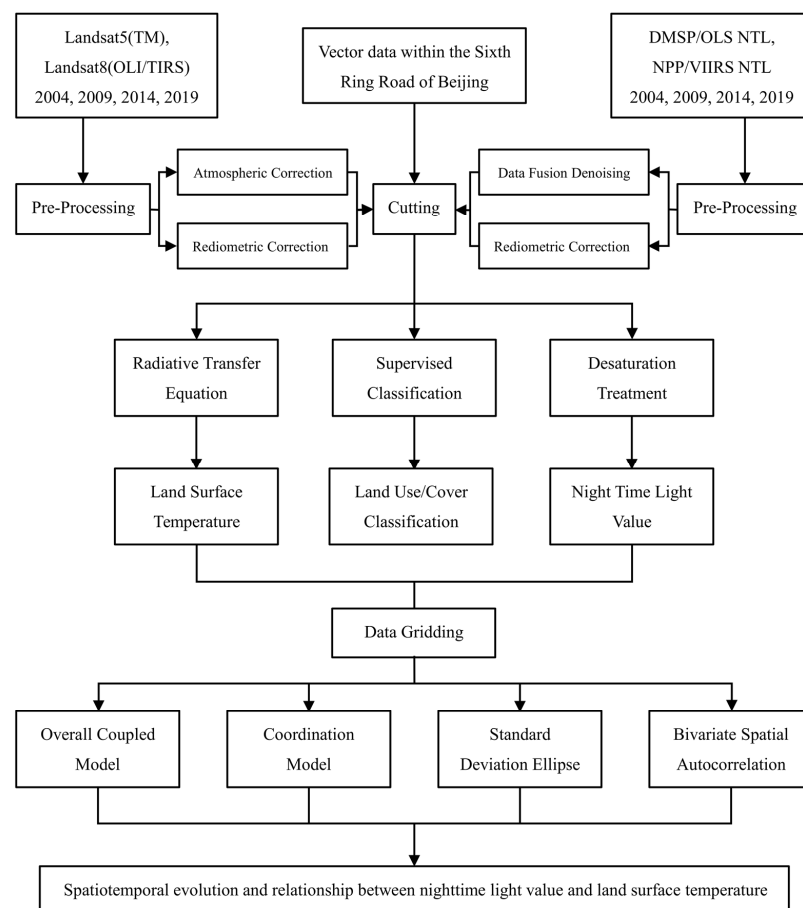


Figure 2. Flow chart of the methodological.

2.3.1. Retrieval of LST

The radiative transfer equation [65,66] was applied to invert the LST through the thermal infrared band in the Landsat images.

First, the surface-specific emissivity was calculated using *NDVI*, which is calculated as follows [67]:

$$P_V = [(NDVI - NDVI_{min}) / (NDVI_{max} - NDVI_{min})]^2 \quad (1)$$

$$\begin{cases} \varepsilon_v = 0.9625 + 0.0614 \times P_V - 0.0461 \times P_V^2 \\ \varepsilon_b = 0.9589 + 0.0860 \times P_V - 0.0671 \times P_V^2 \\ \varepsilon_w = 0.9950 \end{cases} \quad (2)$$

where P_V is the proportion of vegetation in the mixed pixel. *NDVI* is the normalized differential vegetation index. $NDVI_{min}$ and $NDVI_{max}$ are the normalized vegetation index values of bare soil and vegetation, respectively, and take the values of 0.05 and 0.70, respectively [67]. ε_v , ε_b , and ε_w are the specific emissivities of natural surface, construction land, and water bodies, respectively, where 'natural surface' is a mixed image element composed of vegetation and bare soil and 'construction land' is a mixed image element consisting of impervious surfaces, vegetation, and bare soil [36].

Next, the corresponding radiative brightness (L_λ) was calculated from the image element values of the thermal infrared band in the Landsat data. Then, the brightness temperature (T_s) was calculated and converted to LST as follows:

$$L_\lambda = M_L \times DN + A_L \quad (3)$$

$$B(T_s) = [L_\lambda - L_{up} - \tau \times (1 - \varepsilon) \times L_{down}] / (\varepsilon \times \tau) \quad (4)$$

$$T_s = K_2 / \ln \left[\frac{K_1}{B(T_s)} + 1 \right] \quad (5)$$

where $B(T_s)$ denotes the blackbody thermal radiation brightness; T_s denotes the surface temperature; DN is the image element value of the thermal infrared band; and M_L and A_L are the slope and gain of the radiometric calibration of the thermal infrared band, respectively. L_{up} and L_{down} represent the upward and downward radiation brightness of the atmosphere, respectively, and K_1 and K_2 are constants.

The L_{up} , L_{down} , K_1 , and K_2 values for Landsat 5 TM thermal infrared band 6 were 0.38 W/(m²·sr·μm), 3.65 W/(m²·sr·μm), 607.76, and 1260.56, respectively. The L_{up} , L_{down} , K_1 , and K_2 values for Landsat 8 OLI thermal infrared band 10 were 1.25 W/(m²·sr·μm), 2.37 W/(m²·sr·μm), 774.89, and 1321.08, respectively.

The accuracy of the inversion results was verified by studying the LST of the corresponding dates measured at the meteorological stations in the region. These data were obtained from the database of daily values of Chinese terrestrial climate data (<http://data.cma.cn/>, accessed on 6 October 2021). It was found that the absolute errors between the inverse LST and the measured LST were less than 3.42 °C, and the relative errors were less than 15%. In addition, the Pearson correlation coefficients of the inverse LST and the measured LST were all higher than 0.768, and all correlation analysis results passed the significance test at the 0.01 level. Therefore, the inversion results meet the accuracy requirements of the study.

Using the standard deviation method [68], the study area was divided into seven thermal class zones based on LST: extremely high temperature, high temperature, relatively high temperature, medium temperature, relatively low temperature, low temperature, and extremely low temperature. Since the LST values in the extremely high temperature, high temperature, relatively high temperature, and medium temperature zones of the study area are generally higher than the average LST, these areas were considered as urban heat island zones [63].

2.3.2. Data Gridding

Considering the spatial resolution of NTL data and related research results [36,69,70], the study area was divided into 1×1 km grid cells using ArcGIS 10.2 software. The NTL in each grid cell was extracted, and the average LST value in each grid cell was regarded as the LST of that grid cell to realize the unification of the two kinds of data. Finally, the LST and NTL were normalized using the polar difference normalization method, and a map was produced using the formula operation and the interpolation method.

2.3.3. Overall Coupling Model

The overall coupling model measures the coupling of the evolution of spatial variables by comparing the similarities in the distance and the moving direction of the weighted centers of different spatial variables. The smaller the distance between the weighted centers of the spatial variable and the smaller the included angle of the moving trajectory of the weighted centers, the higher the overall coupling of the two variables. The overall coupling model [56] can be calculated as follows:

$$C_{NTL,t}(X_{NTL,t}, Y_{NTL,t}) = \left(\frac{\sum_{i=1}^n m_{NTL,ti} X_{NTL,ti}}{\sum_{i=1}^n m_{NTL,ti}}, \frac{\sum_{i=1}^n m_{NTL,ti} Y_{NTL,ti}}{\sum_{i=1}^n m_{NTL,ti}} \right) \quad (6)$$

$$C_{LST,t}(X_{LST,t}, Y_{LST,t}) = \left(\frac{\sum_{i=1}^n m_{LST,ti} X_{LST,ti}}{\sum_{i=1}^n m_{LST,ti}}, \frac{\sum_{i=1}^n m_{LST,ti} Y_{LST,ti}}{\sum_{i=1}^n m_{LST,ti}} \right) \quad (7)$$

$$L = \sqrt{(X_{LST,t} - X_{NTL,t})^2 + (Y_{LST,t} - Y_{NTL,t})^2} \quad (8)$$

$$\alpha = \arccos \left(\frac{\Delta X_{LST} \times \Delta X_{NTL} + \Delta Y_{LST} \times \Delta Y_{NTL}}{\sqrt{(\Delta X_{LST}^2 + \Delta Y_{LST}^2) \times (\Delta X_{NTL}^2 + \Delta Y_{NTL}^2)}} \right) \times \pi \quad (9)$$

where $C_{NTL,t}$ is the weighted center of the NTL, $C_{LST,t}$ is the weighted center of the LST, $X_{NTL,t}$ and $Y_{NTL,t}$ are the coordinates of the NTL weighted center in period t , $X_{LST,t}$ and $Y_{LST,t}$ are the coordinates of the LST weighted center in period t , $m_{NTL,ti}$ is the value of the NTL in pixel i of period t , $m_{LST,ti}$ is the value of the LST in pixel i of period t , L is the spatial distance between the weighted center of the NTL and LST in period t , and α is the included angle of moving trajectory of the weighted center of LST and NTL in a certain period of time. ΔX_{LST} and ΔY_{LST} and ΔX_{NTL} and ΔY_{NTL} represent the changes in the weighted center coordinates of LST and NTL, respectively, compared with the previous period.

2.3.4. Coordination Model

The coordination model reflects the degree of coordination of the development and evolution of the two variables. A coordination model was used to quantitatively reflect the coordination level between NTL and LST, and the specific classification is shown in Table 2. The calculation [58] is as follows:

$$O = \frac{|(UR + TR)/\sqrt{2}|}{\sqrt{UR^2 + TR^2}} \quad (10)$$

where O is the coordination coefficient of NTL and LST, and UR and TR are the average annual growth rates of NTL and LST, respectively.

Table 2. Classification of coordinated change types between NTL and LST.

Category	Formation Conditions	Meaning
Coordinated enhancement type	$0.8 < O \leq 1.0, UR \approx TR > 0$	The coordination degree of NTL and LST is high, urban development and LST are coordinated enhanced
Antagonistic heating advance type	$0 \leq O < 0.5, TR > UR$	The coordination degree of NTL and LST is low, LST increases ahead of urban development
Running-in heating advance type	$0.5 \leq O < 0.8, TR > UR$	NTL and LST are barely coordinated, LST increases ahead of urban development
Running-in heating hysteresis type	$0.5 \leq O < 0.8, TR < UR$	NTL and LST are barely coordinated, and LST increase lags behind urban development
Antagonistic heating hysteresis type	$0 \leq O < 0.5, TR < UR$	The coordination degree between NTL and LST is low, and LST increase lags behind urban development
Coordinated decline type	$0.8 < O \leq 1.0, UR \approx TR < 0$	The coordination degree of NTL and LST is high, urban development, and LST decrease in coordination

2.3.5. Standard Deviation Ellipse (SDE)

The SDE was first proposed by Lefever in 1926 [59], and with the rapid development of GIS technology, the SDE method based on geographic information has become a conventional statistical tool for spatial statistics modules [71]. In this study, a two-dimensional scatter plot including NTL data on the x -axis and LST data on the y -axis was constructed, and the SDE was used to identify relatively clustered regions and describe the correlation between NTL and LST.

2.3.6. Bivariate Spatial Autocorrelation

Spatial autocorrelation analysis reveals whether the distribution of spatial variables is related to neighboring variables. Bivariate spatial autocorrelation analysis proposed by Anselin effectively reflects the correlation and dependence of the spatial distribution of the two types of variables [60].

3. Results

3.1. Spatiotemporal Coupling Correlation between Urban Development and the LST

This section first analyzed the spatial distribution pattern of NTL and LST within the sixth ring road of Beijing from 2004 to 2019 and then investigated the spatiotemporal coupling relationship between NTL and LST using the overall coupling model and the coordination model. The overall coupling model can be used to analyze the level of coordination among variables, the coordination model can capture the degree of coordination in the evolution of two variables. These two methods are thus more appropriate to reveal the spatiotemporal coupling laws of NTL and LST.

3.1.1. Urban Development and Spatial Distribution Pattern of the Thermal Environment

The spatial distribution of NTL within the sixth ring road of Beijing from 2004 to 2019 shows that high NTL values were concentrated in the central part of Beijing, where dense populations and dense traffic road networks occur (Figure 3). The areas with high NTL values showed a polycentric irregular clustering distribution in 2004 and 2009 and central clustering and diffusion along the traffic road network in 2014 and 2019.

Table 3 shows that, in 2004, 27.56% of the study area was characterized by high NTL values, which were concentrated in the central part of the study area. The average NTL value within the sixth ring road of Beijing was 15.51, with high values concentrated in the western part of the Chaoyang District, southern part of the Haidian District and the eastern part of the Fengtai District. Low values were concentrated in the northern Haidian, eastern Chaoyang, northern Changping, and southern Daxing districts. The highest value, 91.83, was observed in the southeast part of the Chaoyang District in 2004.

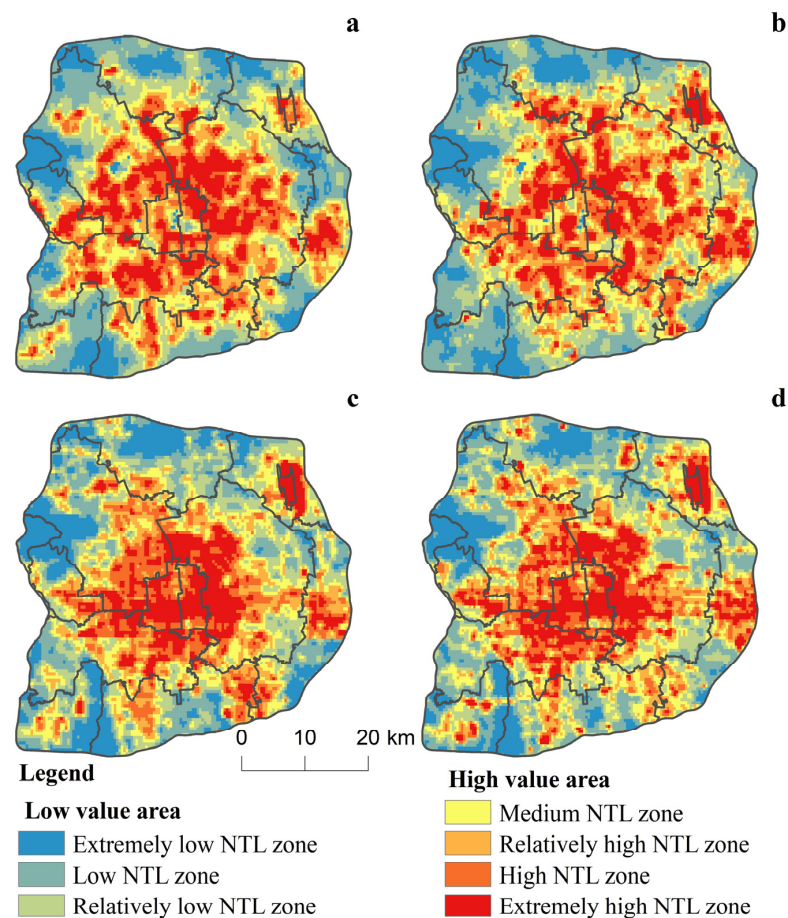


Figure 3. Spatial distribution of NTL within the sixth ring road of Beijing in: (a) 2004, (b) 2009, (c) 2014, (d) 2019.

Table 3. Proportions of areas with high and low NTL values in each administrative region within the sixth ring road of Beijing from 2004 to 2019.

Type	2004		2009		2014		2019	
	Low Value Area	High Value Area						
Changping	13.18	3.60	13.08	4.58	13.91	1.30	13.01	2.75
Chaoyang	15.19	34.52	13.72	36.52	17.65	28.42	17.74	29.31
Daxing	11.89	7.24	13.14	4.66	11.9	7.06	12.76	3.81
Dongcheng	0.82	4.74	1.16	3.64	0.30	6.29	0.68	5.75
Fangshan	7.46	1.08	8.08	0.11	7.33	1.24	6.98	1.66
Fengtai	10.17	15.68	10.74	13.91	10.51	14.91	10.19	16.40
Haidian	15.55	19.37	17.33	14.88	15.85	18.66	16.9	15.66
Mentougou	1.77	0.06	1.85	0.00	1.77	0.00	1.71	0.00
Shijingshan	3.80	3.39	4.07	2.76	3.98	2.86	3.71	3.60
Shunyi	7.70	1.51	6.46	4.89	6.61	4.29	6.12	5.57
Tongzhou	10.67	5.39	8.82	10.15	9.94	7.25	9.56	8.15
Xicheng	1.80	3.42	1.55	3.90	0.25	7.72	0.64	7.34
Sum	100.00	100.00	100.00	100.00	100.00	100.00	100.00	100.00

In 2009, the number of areas with high NTL values was higher than that in 2004, accounting for 29.84% of the study area. The average NTL value in the study area was 21.09. After 2004, the speed of urban development within the sixth ring road of Beijing accelerated, and the Chaoyang, Haidian, and Fengtai districts were greatly developed.

Therefore, high NTL values were still concentrated in these regions and the proportion of each district slightly increased. Owing to the Beijing Olympic Games, the proportion of the Tongzhou District increased, and the district became an area with high NTLs. Except for the Tongzhou District, areas with low NTL values insignificantly changed. The highest NTL value in the study area, 129.67, was observed in the south of the Shunyi District.

In 2014, the area with high NTL values had decreased, accounting for 26.70% of the study area; the average value was 17.89. The high NTL values were still concentrated in the Chaoyang, Haidian, and Fengtai districts. The proportion of area with high NTL values in the Chaoyang District significantly decreased and that of the rest of the districts slightly increased. The area with high NTL values in the Xicheng and Dongcheng districts doubled. The area with low NTL values in the study area remained stable. The highest NTL value (255.27) was observed in the northeast of the Chaoyang District.

In 2019, the area with high NTL values decreased compared with that in 2014, accounting for 24.06% of the study area; the average value was 21.93. The distribution of high NTL values remained unchanged. The proportion of area with high NTL values in the Haidian District slightly decreased and that of the Chaoyang and Fengtai districts slightly increased. The area with low NTL values remained stable. The highest NTL value (381.49) was observed at the junction of the Dongcheng and Xicheng districts.

The heat island areas within the sixth ring road in Beijing from 2004 to 2019 showed a polycentric irregular clustering distribution, and the four temperature zones representing heat islands were concentrated in built-up urban areas with dense buildings and populations (Figure 4).

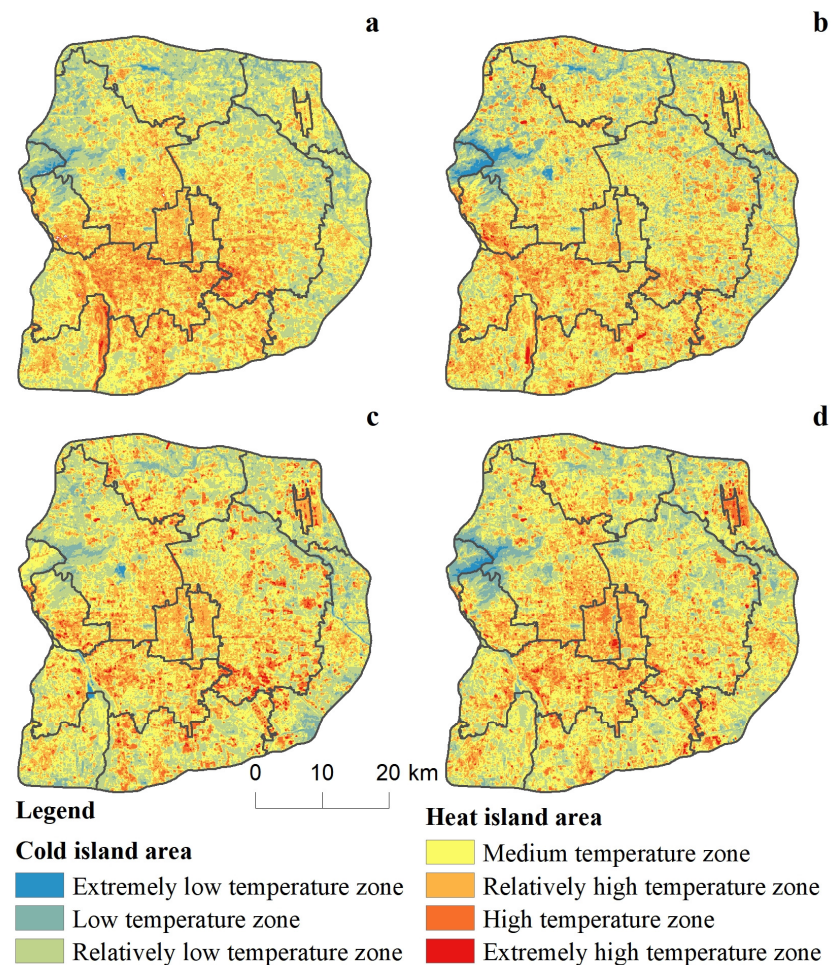


Figure 4. Distribution of the thermal grade within the sixth ring road of Beijing in: (a) 2004, (b) 2009, (c) 2014, (d) 2019.

Table 4 shows that, in 2004, the heat island area was relatively small and concentrated in the central and southwestern parts within the sixth ring road in Beijing (Chaoyang, Fengtai, Haidian, and Daxing districts). The mean surface temperature of the heat island area in 2004 was 32.898 °C. The cold island areas were concentrated in the Haidian, Chaoyang, Changping, and Tongzhou districts. In 2004, the highest and lowest surface temperatures within the sixth ring road in Beijing were 41.02 and 21.22 °C, respectively, representing a difference of 19.8 °C.

Table 4. Proportions of cold and heat islands within the sixth ring road of Beijing from 2004 to 2019.

Type	2004		2009		2014		2019	
	Cold Island Area	Heat Island Area						
Changping	18.07	7.04	14.72	8.85	12.20	9.84	13.01	9.51
Chaoyang	18.45	21.44	21.13	20.17	17.06	22.25	20.05	20.67
Daxing	3.98	13.99	5.24	13.12	10.06	11.06	8.75	11.65
Dongcheng	0.41	2.55	1.19	2.15	0.53	2.54	0.49	2.51
Fangshan	4.13	6.53	3.85	6.58	7.17	5.00	5.78	5.73
Fengtai	2.98	15.97	5.36	14.52	6.49	14.44	6.19	14.37
Haidian	20.39	14.34	20.64	14.42	18.72	15.07	18.35	15.35
Mentougou	3.28	0.41	3.38	0.45	1.71	1.16	3.55	0.29
Shijingshan	3.27	3.92	3.52	3.79	2.92	4.11	4.10	3.51
Shunyi	10.90	3.57	8.96	4.65	8.91	4.43	8.50	4.75
Tongzhou	13.78	7.11	10.96	8.55	13.74	6.96	10.81	8.56
Xicheng	0.36	3.13	1.05	2.75	0.49	3.14	0.42	3.10
Sum	100.00	100.00	100.00	100.00	100.00	100.00	100.00	100.00

In 2009, the heat island area expanded compared with 2004, and the mean surface temperature in the heat island area was 27.959 °C. After 2004, the speed of urban development of the study area accelerated and the Chaoyang, Fengtai, Haidian, and Daxing districts were greatly developed. Therefore, heat islands were still mainly concentrated in these areas, the proportion of each district insignificantly changed, and the spatial location of the heat island area changed. Cold island areas were concentrated in the Chaoyang, Haidian, Changping, and Tongzhou districts. The spatial location of cold island areas insignificantly changed. The proportion of cold island areas in the Chaoyang District increased, while that in the Changping and Tongzhou districts decreased and that in the Haidian District insignificantly changed. In 2009, the highest and lowest surface temperatures within the sixth ring road of Beijing were 51.96 and 15.76 °C, respectively, representing a difference of 28.52 °C.

The Beijing Municipal Government Report 2010 points out that Beijing's environmental problems require urgent attention. It introduces strict control policies, such as total population control and traffic restrictions, as well as measures to protect water sources and strengthen planning constraints. It appears to have achieved some results: The heat island area slightly decreased in 2014. The heat island areas were still concentrated in the Chaoyang, Fengtai, Haidian, and Daxing districts. The proportion of the heat island area in the Chaoyang District to the total heat island area slightly increased, while in the Daxing District, it slightly decreased and in the Fengtai and Haidian districts, it remained stable. Cold island areas were concentrated in the Haidian, Chaoyang, Tongzhou, Changping, and Daxing districts. The proportion of cold island areas in the Haidian, Chaoyang, and Changping districts to the total cold island area slightly decreased, while that in the Tongzhou and Daxing districts significantly increased.

The area of heat islands in 2019 increased compared with 2014 because of the opposing effects of urban development and ecological protection policies. The heat island areas were still concentrated in the Chaoyang, Fengtai, Haidian, and Daxing districts. The proportion of the heat island area in the Chaoyang District to the total heat island area slightly decreased, while it remained stable in the other districts. Cold island areas were concentrated in the Chaoyang, Haidian, Changping, and Tongzhou districts. The proportion of cold

island areas in the Chaoyang and Changping districts to the total cold island area slightly increased, while that in the Tongzhou, Daxing, and Haidian districts slightly decreased.

In summary, the LST strongly correlates with urban development. The highest temperatures of the study area were observed in the urban development zone. Lower temperatures were mainly recorded in rivers, inner lakes, and high mountains, as well as in less-developed areas at the edge of the city. According to the comparison of the four-phase time series diagram of the NTL and thermal class, the extension direction of the heat island area from 2004 to 2019 is the same as that of the built-up area.

3.1.2. Spatiotemporal Coupling of the NTL and LST

The coupling degree of the NTL and LST of the study area was measured using the overall coupling model (Figure 5 and Table 5). Overall, during 2004 to 2019, the distance between the weighted centers of the NTL and LST and the angle between the moving directions of the weighted centers initially increased significantly and then decreased, with an overall small increase. The overall coupling first significantly weakened and then continuously strengthened. The moving direction of the weighted centers of the NTL and LST was overall identical, but their directions were opposite in the late stage. From 2004 to 2009, the northeastern part of the study area, Chaoyang and Shunyi, had higher urban construction rates due to the Olympic Games, resulting in a shift in the weighted center of NTL to the northeast and a significant shift in the weighted center of LST. From 2009 to 2014, the moving direction of the weighted center of the NTL was the same as the direction of urban construction in Beijing, which still moved toward the northeast of the study area. At the same time, the weighted center of the LST shifted toward southwestern Beijing because of the UHI effect driven by the event activities weakened after the Beijing Olympic Games. The development of Daxing and Tongzhou districts in the southeast of the study area from 2014 to 2019 caused the weighted center of the NTL to move to the southeast, whereas the weighted center of the LST moved to the northeast in the same direction as the weighted center of the NTL from 2009 to 2014 because the effect of the urban development on the LST is hysteretic.

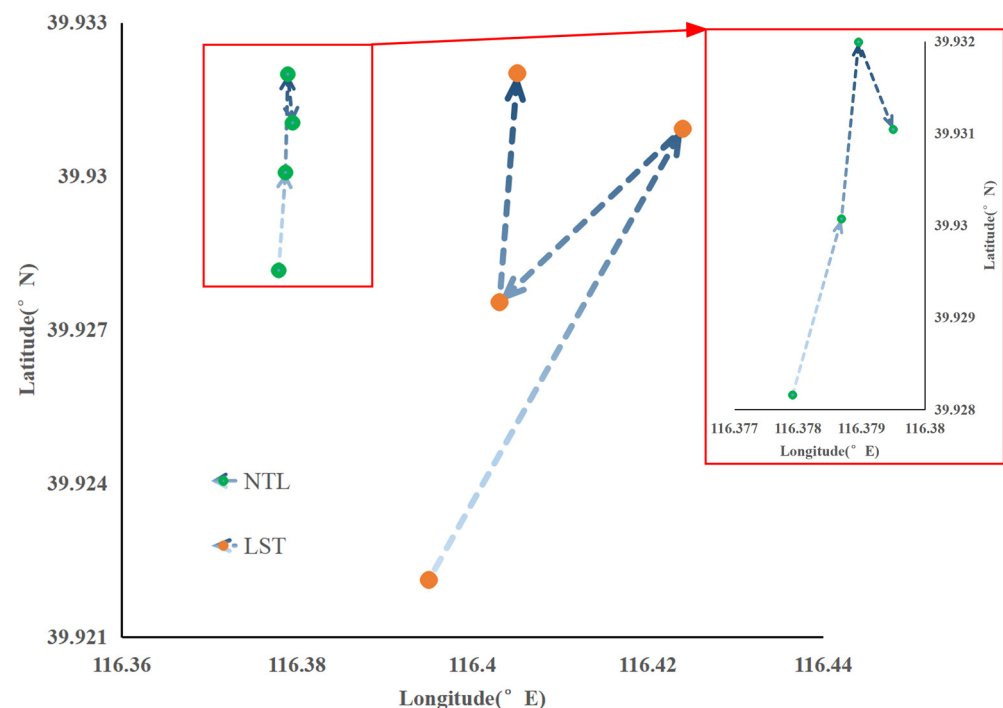


Figure 5. Trajectory of the LST and NTL weighted center within the sixth ring road of Beijing from 2004 to 2019.

Table 5. Coupling analysis of the LST and NTL within the sixth ring road of Beijing from 2004 to 2019.

Year	Distance between Weighted Centers (km)	Period	Angle of the Moving Direction of the Weighted Center (°)
2004	1.609	2004–2009	47.498
2009	3.872	2009–2014	160.812
2014	2.119	2014–2019	159.678
2019	2.190	2004–2019	70.305

3.1.3. Spatial Coordination Characteristics of the NTL and LST

Table 6 shows that the area of each coordination type of the NTL and LST of the study area varied widely in different periods. The area of coordinated enhancement, coordinated decline, and antagonistic heating hysteresis continued to decrease, whereas that of antagonistic heating advance and running-in heating advance continued to increase. The area of running-in heating hysteresis first increased and then decreased, with an overall decreasing trend. The coordination types of the NTL and LST of the research area in all three time periods showed an irregular circular distribution.

Table 6. Areas and proportions of coordination types between NTL and LST within the sixth ring road of Beijing from 2004 to 2019.

Year	Coordinated Enhancement Type		Antagonistic Heating Advance Type		Running-In Heating Advance Type		Running-In Heating Hysteresis Type		Antagonistic Heating Hysteresis Type		Coordination Decline Type	
	Area (km ²)	Proportion (%)	Area (km ²)	Proportion (%)	Area (km ²)	Proportion (%)	Area (km ²)	Proportion (%)	Area (km ²)	Proportion (%)	Area (km ²)	Proportion (%)
2004–2009	207.06	9.13	217.81	9.60	432.16	19.06	514.87	22.70	514.49	22.68	381.69	16.83
2009–2014	40.68	1.79	320.67	14.14	583.57	25.73	563.61	24.85	392.63	17.31	366.92	16.18
2014–2019	36.27	1.60	782.77	34.51	676.84	29.84	366.34	16.15	218.00	9.61	187.87	8.29

Figure 6 shows that from 2004 to 2009, the coordination type in the central part of the study area was mainly coordination decline due to the Olympic events. The proportions of the running-in heating hysteresis and antagonistic heating hysteresis types were the largest, together accounting for 45.38% of the study area. They were mainly distributed in the Xicheng, Dongcheng, southern Haidian, western Chaoyang, and northern Fengtai districts. The running-in heating advance was concentrated in the northern part of the research area and the coordinated enhancement was concentrated in the eastern part. The coordination decline, antagonistic heating hysteresis, running-in heating hysteresis, running-in heating advance, antagonistic heating advance, and coordinated enhancement types within the sixth ring road of Beijing showed a circular distribution from the center to the periphery.

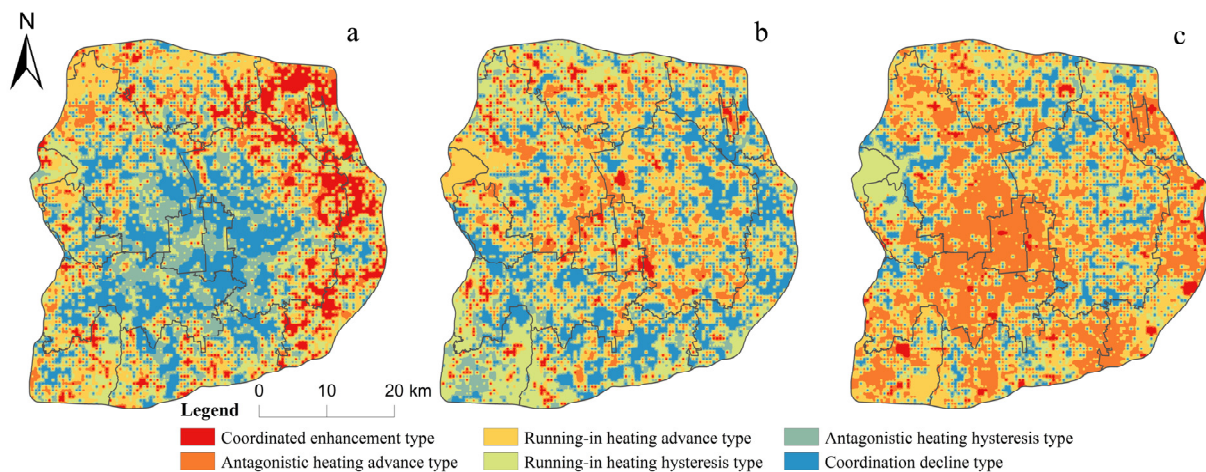


Figure 6. Distribution of coordination types between NTL and LST changes within the sixth ring road of Beijing from: (a) 2004 to 2009, (b) 2009 to 2014, (c) 2014 to 2019.

From 2009 to 2014, the main coordination type in the central part within the sixth ring road of Beijing was coordinated enhancement, but the proportion was small, accounting for only 1.79% of the research area. The antagonistic heating advance type was concentrated in the southern Haidian and western Chaoyang districts. The proportions of the running-in heating advance and running-in heating hysteresis types were the largest, together accounting for 50.58% of the research area. The two types were mainly located in peripheral areas such as the Fangshan, Changping, Daxing, Tongzhou, northern Haidian, and Mentougou districts. The coordinated enhancement, antagonistic heating advance, running-in heating advance, coordination decline, antagonistic heating hysteresis, and running-in heating hysteresis types in the study area presented a circular distribution from the center to the periphery.

From 2014 to 2019, the main coordination type in the central part within the sixth ring road of Beijing was antagonistic heating advance. This type was concentrated in the Xicheng, Dongcheng, Eastern Fengtai, and eastern Haidian districts. The proportions of the antagonistic heating advance and running-in heating advance types were the largest, accounting for 64.35% of the study area. The hysteresis type running-in heating was mainly distributed in the Mentougou District and northern part of the Shijingshan District. The antagonistic heating advance, running-in heating advance, coordination decline, antagonistic heating hysteresis, running-in heating hysteresis, and coordinated enhancement types in the study area presented a circular distribution from the center to the periphery.

Table 7 shows that the proportion of coordination types in the study area continued to decrease. From 2004 to 2009, the coordinated enhancement type was mainly distributed in the Chaoyang, Tongzhou, and Shunyi districts, accounting for 31.14%, 28.08%, and 24.19%, respectively. From 2009 to 2014, it was mainly distributed in the Chaoyang and Changping districts, accounting for 25.94% and 23.11%, respectively. From 2014 to 2019, this type was mainly distributed in the Tongzhou District, accounting for 33.86%. In the 2004 to 2009 time period, the coordination decline type was mainly distributed in the Chaoyang, Fengtai, and Haidian districts, accounting for 29.46%, 19.66%, and 15.84%, respectively. From 2009 to 2014, it was mainly distributed in the Chaoyang and Tongzhou districts, accounting for 27.88% and 20.35%, respectively. In the 2014 to 2019 time period, this type was mainly distributed in the Chaoyang and Changping districts, accounting for 45.05% and 16.34%, respectively.

Figure 7 shows that the proportion of the antagonistic type first remained stable and then significantly increased. The antagonistic heating advance type was mainly distributed in the Chaoyang and Changping districts during the 2004 to 2009 period, accounting for 20.97% and 16.92%, respectively. From 2009 to 2014, it was mainly distributed in the Chaoyang and Haidian districts, accounting for 31.12% and 21.24%, respectively. From 2014 to 2019, it was mainly distributed in the Haidian, Fengtai, and Chaoyang districts, accounting for 18.83%, 16.45%, and 16.08%, respectively. The antagonistic heating hysteresis type was mainly distributed in the Haidian, Chaoyang, and Fengtai districts in the 2004 to 2009 period, accounting for 20.36%, 20.18%, and 17.57%, respectively; in the Fengtai District in the 2009 to 2014 time period, accounting for 18.08%; and in the Chaoyang, Haidian, and Daxing districts, accounting for 22.18%, 18.40%, and 15.85%, respectively.

The proportion of the running-in type first increased and then decreased. The running-in heating advance type was mainly distributed in the Changping and Haidian districts in the 2004 to 2009 period, accounting for 20.12% and 19.23%, respectively. It was mainly distributed in the Chaoyang and Haidian districts from 2009 to 2014, accounting for 24.79% and 20.95%, respectively. From 2014 to 2019, this type was concentrated in the Chaoyang and Haidian districts, accounting for 21.27% and 15.17%, respectively. The running-in heating hysteresis type was concentrated in the Haidian and Chaoyang districts from 2004 to 2009, accounting for 18.82% and 16.32%, respectively. From 2009 to 2014, it was mainly distributed in the Fengtai District, accounting for 15.02%. From 2014 to 2019, it was mainly distributed in the Haidian District, accounting for 17.60%.

Table 7. Proportions of coordination types between NTL and LST within the sixth ring road of Beijing.

Types	Coordinated Enhancement Type			Antagonistic Heating Advance Type			Running-In Heating Advance Type		
	04–09	09–14	14–19	04–09	09–14	14–19	04–09	09–14	14–19
Changping	10.19	23.11	12.7	16.92	11.61	6.57	20.12	12.04	12.02
Chaoyang	31.14	25.94	6.35	20.97	31.12	16.08	12.39	24.79	21.27
Daxing	1.48	0.47	4.23	8.99	5.21	9.68	11.41	6.51	11.14
Dongcheng	0.00	8.96	2.65	0.00	3.23	3.87	0.13	2.66	1.36
Fangshan	1.67	6.13	12.17	7.84	1.92	4.34	8.21	1.48	9.05
Fengtai	0.84	9.44	6.88	5.55	6.82	16.45	7.28	7.40	10.60
Haidian	1.76	7.55	4.23	12.16	21.24	18.83	19.23	20.95	15.17
Mentougou	0.28	0.00	1.06	1.58	0.42	0.10	2.00	4.21	0.20
Shijingshan	0.37	1.89	1.06	2.73	3.59	2.04	4.80	4.24	2.55
Shunyi	24.19	8.49	11.64	11.28	6.22	5.20	4.31	5.95	5.87
Tongzhou	28.08	4.25	33.86	11.89	4.61	11.08	9.86	7.14	10.29
Xicheng	0.00	3.77	3.17	0.09	4.01	5.76	0.26	2.63	0.48

Types	Running-in Heating Hysteresis Type			Antagonistic Heating Hysteresis Type			Coordination Decline Type		
	04–09	09–14	14–19	04–09	09–14	14–19	04–09	09–14	14–19
Changping	9.77	12.84	12.47	5.97	7.97	12.68	4.07	5.7	16.34
Chaoyang	16.32	8.78	16.08	20.18	14.57	22.18	29.46	27.88	45.05
Daxing	14.16	14.74	12.68	11.04	14.61	15.85	10.11	12.24	3.47
Dongcheng	0.82	1.06	0.47	3.02	1.66	0.35	5.93	0.26	0.00
Fangshan	7.72	11.34	3.98	3.54	9.09	5.19	3.87	3.24	1.74
Fengtai	10.62	15.02	9.06	17.57	18.08	9.86	19.66	11.14	4.09
Haidian	18.82	19.2	17.60	20.36	14.47	18.40	15.84	4.60	10.21
Mentougou	2.39	0.24	7.23	0.75	0.15	0.35	0.25	0.52	0.00
Shijingshan	4.03	3.95	9.22	5.00	2.83	5.28	2.46	3.50	2.35
Shunyi	4.58	3.47	6.29	3.10	5.23	5.19	0.91	10.36	9.19
Tongzhou	9.06	7.25	4.56	4.47	9.19	4.67	3.52	20.35	7.56
Xicheng	1.71	2.11	0.36	5.00	2.15	0.00	3.92	0.21	0.00

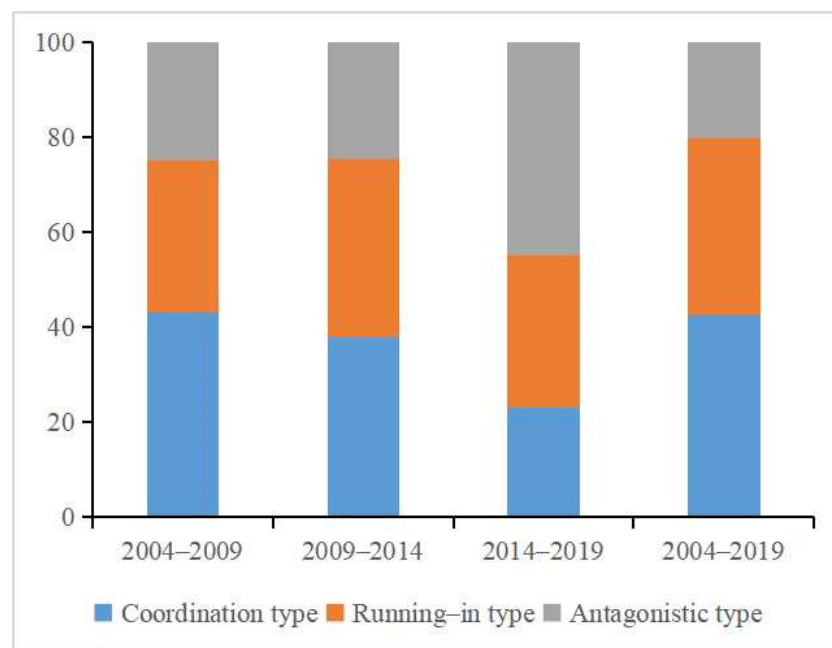


Figure 7. Proportions of the coordination types between NTL and LST within the sixth ring road of Beijing from 2004 to 2019.

3.2. Influence Mechanism of NTL on LST

This section focused on the interrelationship between NTL and LST from 2004–2019 within the sixth ring of Beijing using standard deviation ellipses and bivariate spatial autocorrelation. The standard deviation ellipse can reflect the degree of concentration and dominant direction of the spatial pattern of variables, and bivariate spatial autocorrelation can effectively reflect the association and dependence characteristics of the spatial distribution of two types of variables. These two techniques can be used to explore the spatial response law between NTL and LST.

3.2.1. Correlation between NTL and LST

In this study, we used the SPSS software to calculate the correlation coefficients between the NTL and LST data and analyzed the changes in spatial characteristics of the two-dimensional scatter of the NTL and LST data using SDE (Table 8 and Figure 8). The results showed that from 2004 to 2019, the NTL and LST of the research area were significantly and positively correlated. The directionality of the SDE was notable and less discrete, which indicates that an increase in NTL leads to an increase in the LST. This correlation was due to the broad replacement of natural to impermeable surfaces caused by urban development; urban buildings impeded ventilation and heat dissipation. Under the combined effect of various factors, the LST had increased.

Table 8. Relevant NTL and LST parameters within the sixth ring road of Beijing from 2004 to 2019.

Year	Correlation Coefficient ¹	Standard Deviation Elliptic Parameter		
		Center of Inertia (NTL, LST)	Azimuth (°)	Oblateness
2004	0.425 **	(0.199, 0.478)	50.531	0.370
2009	0.211 **	(0.265, 0.498)	75.837	0.357
2014	0.354 **	(0.231, 0.443)	48.094	0.311
2019	0.427 **	(0.264, 0.453)	59.444	0.403

¹ ** denotes that the correlation was significant at the level of 0.01 (detection < 0.01).

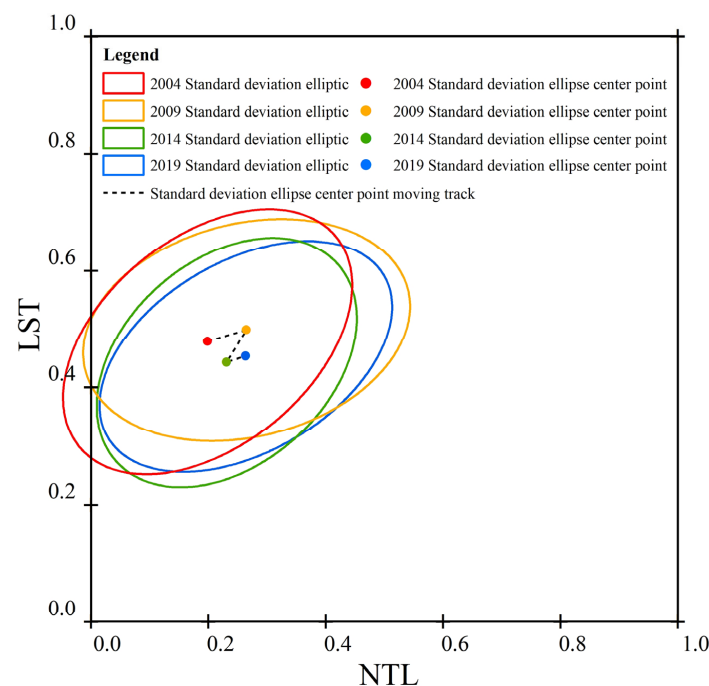


Figure 8. Spatial characteristics of the standard deviation ellipses of the NTL and LST within the sixth ring road of Beijing from 2004 to 2019.

Table 8 shows the positive effect of NTL on the LST of the study area. From 2004 to 2009, the urban development of Beijing accelerated owing to the Olympic Games. The center of the SDE simultaneously moved along the x -axis (NTL) and y -axis (LST) toward the high-value area, which indicates a significant positive effect of the increase in the NTL on the LST. From 2009 to 2014, the center of the SDE simultaneously moved along the x -axis (NTL) and y -axis (LST) toward the low-value area because of ecological protection policies, indicating that the reduction in the LST has a negative effect on the NTL. From 2014 to 2019, the center of the SDE simultaneously moved along the x -axis (NTL) and y -axis (LST) toward the high-value area under the opposing effects of urban development and ecological protection policies, which indicates that the effect of urban development on the LST strengthened and gradually became positive.

3.2.2. Spatial Correlation between NTL and LST

OpenGeoDa software was used to calculate the bivariate Moran's I of the NTL and LST of the research area (Table 9 and Figure 9). The results indicate a significant positive spatial correlation between the NTL and LST within the sixth ring road of Beijing, that is, an increase in the NTL in local areas leads to an increase in the LST in surrounding areas. This correlation is due to the heat exchange between different regions because of the difference in the LST. The local NTL increase drives the increase in the LST in that area. The heat in that area then transfers to the surrounding areas, which eventually leads to an increase in the LST in the surrounding areas. The bivariate Moran's I value of the NTL and LST gradually increased from 2004 to 2019, that is, the positive effect of the NTL on the LST in surrounding areas strengthened. This is due to the expansion of the town area and gradual and continuous concentration of the spatial distribution, resulting in the enhancement of the UHI effect and a significant warming of the surrounding environment.

Table 9. Bivariate Moran's I statistics of the LST and NTL within the sixth ring road of Beijing from 2004 to 2019.

Year	Bivariate Autocorrelation ²
2004	0.403 (100.9594) ***
2009	0.192 (50.6277) ***
2014	0.321 (82.8475) ***
2019	0.354 (92.3110) ***

² *** denotes that the correlation was significant at the level of 0.001 (detection < 0.001).

The "hot spot" (HH)-type refers to high NTL units adjacent to high LST units. The effect of the Olympic Games in 2009 led to an insignificant correlation between the NTL and LST in the central urban area, leading to a significant reduction in the HH area from 2004 to 2019, followed by a continuous increase. The HH-type was mostly clustered in the central areas of the study area (e.g., Xicheng, Dongcheng, southern Haidian, western Chaoyang, and eastern Fengtai districts), which are characterized by a flat topography, developed transportation, dense population, rapid urban construction, and a strong UHI effect. Low NTL units are surrounded by high LST units.

The "cold spot" (LL)-type means that low NTL units are adjacent to low LST units. From 2004 to 2019, the LL area of the research area first decreased, then increased, and then decreased; it was mainly concentrated in the urban fringe areas (e.g., Mentougou, northern Haidian, northern Changping, and western Shunyi districts), which are characterized by high topography, mountainous and forested areas, large lakes, less population, slow urban construction, and a weak UHI effect.

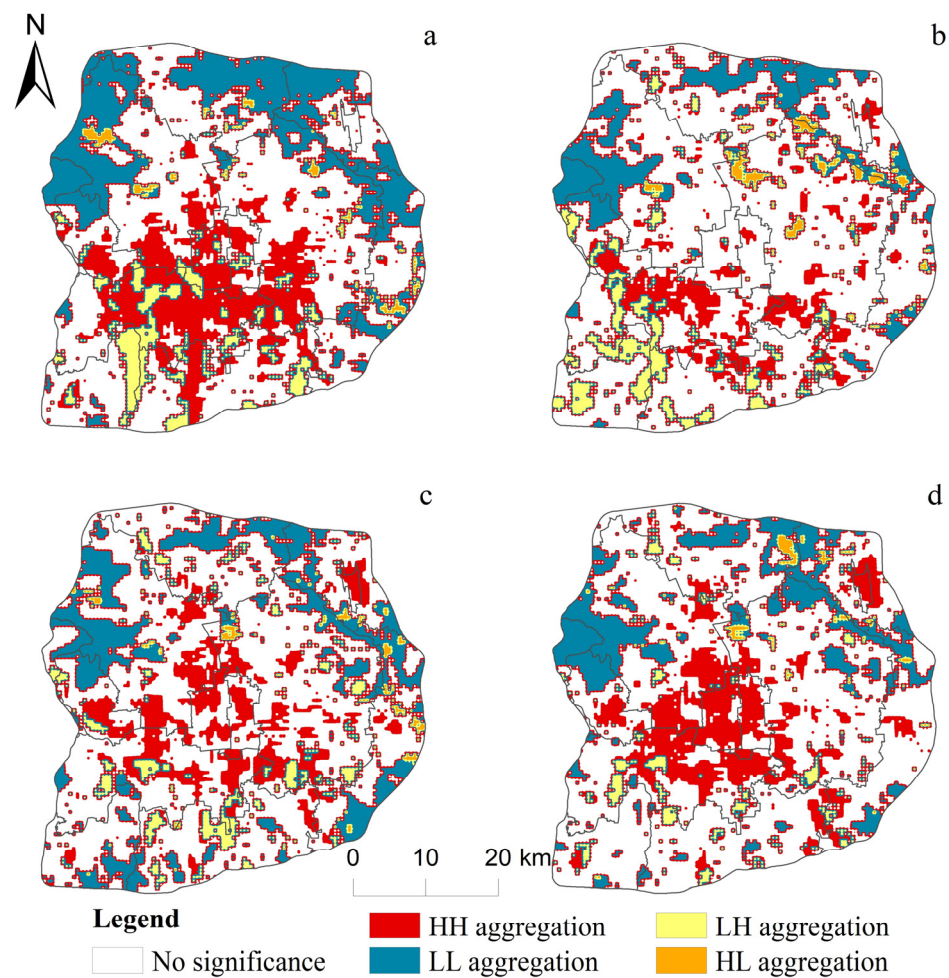


Figure 9. Bivariate Local Indicator for Spatial Autocorrelation distribution of the NTL and LST within the sixth ring road of Beijing in: (a) 2004, (b) 2009, (c) 2014, (d) 2019.

The “heterogeneous point” (LH)-type refers to low NTL units surrounded by high LST units. From 2004 to 2019, the LH area first remained stable and then decreased. It was mostly clustered in the areas around the HH agglomeration (i.e., northern Fangshan, western Daxing, and southern Chaoyang districts), which are mostly large areas with bare land, cultivated land, and industry. Although the NTL is relatively low, the effects of solar radiation or anthropogenic heat emissions lead to a relatively high LST.

The “heterogeneous point” (HL)-type refers to high LST units surrounded by low NTL units. From 2004 to 2019, the HL area first increased and then decreased, and was mainly observed in areas around the LL agglomeration (i.e., northern Haidian, northern Chaoyang, and southern Chaoyang districts), which are near mountains, forests, lakes, and fragmented town areas. Despite the high NTL, the “cold island effect” of the surrounding natural surface leads to a relatively low LST.

4. Discussion

4.1. Correlation between NTL and LST

This study clarifies the spatiotemporal evolution and interrelationship of NTL and LST within the sixth ring road of Beijing. NTL data exceed beyond the limitations of previous index data and make the research results more accurate because they can reflect the spatial development differences and speed within a city [72,73]. The results demonstrate that the spatial distribution of NTL and LST within the sixth ring road of Beijing from 2004 to 2019 was closely related. High temperatures mainly occurred in the central part of the study area with high NTL values, and low temperatures were mainly found at rivers, lakes,

mountains, and less-developed areas. These areas had low NTL values and are located at the edge of the city.

From 2004 to 2019, the distance between the weighted centers of the NTL and LST and the angle between the moving directions of the weighted centers of the research area first significantly increased and then decreased, with an overall small increase. The overall coupling first significantly decreased and then continuously increased. The moving directions of the weighted centers of the NTL and LST were the same in the early stage, opposite in the late stage, and the same overall.

The area of each coordination type of the NTL and LST significantly varied. From 2004 to 2019, the areas of coordinated enhancement, coordination decline, and antagonistic heating hysteresis continued to decrease; the areas of antagonistic heating advance and running-in heating advance continued to increase, and the area of running-in heating hysteresis first increased and then decreased. From the perspective of coordination types, it was mainly heating hysteresis within the sixth ring road of Beijing from 2004 to 2009, accounting for 45.38% of the study area; from 2009 to 2014, it was mainly the running-in, accounting for 50.58% of the study area; from 2014 to 2019, it was mainly the heating advance, accounting for 64.35% of the study area. Most studies of urbanization dynamics and their impact on surface heat islands in the case of Beijing have suggested that with rapid urban expansion, the NTL values first increases rapidly, and then the growth rate slows down [74]. This finding also explains the prominent increase in LST observed during this stage. This shows that the main types of coordination between NTL and LST within the sixth ring road of Beijing deteriorated over time, with LST increases lagging behind NTL from 2004 to 2009 (heating hysteresis type) and LST increased ahead of NTL from 2014 to 2019 (heating advance type). This suggests that urban development became less efficient and LST increases became more significant.

From 2004 to 2019, the NTL and LST of the research area were significantly positively correlated, and the correlation coefficient first decreased significantly and then continued to increase. This result reflects the findings of a previous study on urbanization and the urban heat island effect in Beijing from 1995 to 2009, in which strong evidence that this phenomenon exists in the city is provided [75]. It is suggested again that there is a close relationship between temperature distribution and regional urbanization level. The SDE had a notable directivity and small discreteness, which indicates that an increase in NTL leads to a more rapid increase in LST. Some scholars point out that the impervious surface within the sixth ring road of Beijing expanded significantly from 1997 to 2017 [76]. The replacement of natural surfaces by impermeable surfaces and the obstruction of ventilation and heat dissipation by urban buildings are contributing to the increase in LST [77].

From 2004 to 2009, a period of more prominent urban development, the HH-type area decreased and the HL-type area increased. Across the rest of the study period, the LST increased more significantly than NTL. At the spatial scale, four types of spatial correlation patterns of NTL and LST could be distinguished. The HH aggregation was mostly concentrated in the central areas of the research area with a flat topography, developed transportation, dense population, fast urban construction, strong UHI effect, and a notable trend of expansion and aggregation. The LL aggregation mostly occurred in urban fringe areas with a higher terrain, mountains, forests, or large lakes in which the population was smaller, urban construction was slower, the UHI effect was weaker, and the distribution was relatively stable. The LH aggregation was mostly distributed around the HH aggregations, mainly found in large areas with bare land, cropland, and industry. Although the NTL was relatively low in these areas, LST was relatively high due to solar radiation or anthropogenic heat emission. The HL aggregation area was relatively small and mostly distributed around LL aggregations, mainly near mountain forests, lakes, and fractured urban areas. Although the NTL was relatively high, the LST was relatively low due to the “cold island effects” of surrounding natural surfaces. These findings suggest that urban development becomes less efficient and LST increases more significantly over time, which will greatly affect the urban ecological environment and residents’ health.

4.2. Recommendations for Sustainable Development

The results of this study provide a reference for advancing sustainable urban development. The results show that the efficiency of urban development decreases and LST increases more significantly over time. Therefore, corresponding planning strategies should be developed for cities according to their urbanization stage [78]. For cities at the high level of urbanization stage, due to limited available land, urban landscape configuration should be prioritized. However, simply changing the landscape composition, such as increasing urban green space and limiting impervious surface expansion, is not an effective way to mitigate increases in urban surface temperature. More attention should be paid to various cost-effective means [79], such as road cooling [80–82], urban green roofs [83,84], and the cooling of building materials [85,86]. For cities at the low level of urbanization stage, green spaces should be preserved, which would help improve urban thermal comfort and mitigate surface temperature increases in built-up areas of the city.

At the same time, when planning for different LST areas, specific analysis should be conducted so that corresponding strategies can be determined [87]. For example, in areas where industries are concentrated, optimizing neighborhood space and reducing waste emissions can facilitate decreases in LST; in areas with dense buildings and few green spaces, vertical greening and vegetation density should be increased [88,89], and dilapidated buildings should be demolished to increase air circulation. Stricter greening policies should be implemented in new expansion areas, which, combined with the optimal park cooling range and scale, can help mitigate the urban heat island effect [90].

Finally, in terms of urban planning and management, the main challenge is the implementation of regulations related to sustainable development goals. In response to urban sprawl and the problems caused by extreme weather events, the Beijing Master Plan states that population density should be reduced and total building area should be strictly controlled. In most cases, however, detailed large-scale urban plans are not coordinated with higher-order plans and do not strictly adhere to their strategic goal of protecting green spaces. Instead, the protection of green space is often compromised to satisfy the interests of private stakeholders. The important issue also lies in the lack of measures and instruments for the implementation of green infrastructure principles [91]. Therefore, governments need to enact strict green policy interventions and effective urban planning to control rapidly rising urban temperatures [92].

4.3. Limitations

This study has shortcomings due to the complexity of surface temperature changes and the limited availability of basic research data. First, this study analyzed the spatiotemporal evolution and relationship between NTL and LST for just four years: 2004, 2009, 2014, and 2019. Therefore, further studies are needed to address this aspect by applying the most recent multi-temporal remote sensing data in the future. In addition, because the surface temperature is affected by various factors, such as latitude and longitude, and global climate changes [93], the effects of various factors were not analyzed comprehensively when the relationship between NTL and LST was explored. Finally, the spatial resolution of the remote sensing data must be improved by using higher-resolution remote sensing data in the future.

5. Conclusions

- (1) From the perspective of spatiotemporal evolution, the spatial distribution of NTL and LST within the sixth ring road of Beijing from 2004 to 2019 was closely related. High temperatures mainly occurred in urban development zones with high NTL values, and low temperatures mainly occurred in less-developed areas with low NTL values. From 2004 to 2019, the overall coupling of NTL and LST first significantly weakened and then continuously strengthened. The moving directions of the weighted centers of the NTL and LST were the same in the early stage, then opposite in the late stage; however, overall, they were the same.

- (2) From the perspective of coordination types, it was mainly heating hysteresis within the sixth ring road of Beijing from 2004 to 2009, accounting for 45.38% of the study area; from 2009 to 2014, it was mainly the running-in, accounting for 50.58% of the study area; from 2014 to 2019, it was mainly the heating advance, accounting for 64.35% of the study area. This shows that the main types of coordination between NTL and LST within the sixth ring road of Beijing deteriorated over time, with LST increased lagged behind NTL from 2004 to 2009 (heating hysteresis type) and LST increased ahead of NTL from 2014 to 2019 (heating advance type). This suggests that urban development became less efficient and LST increases became more significant.
- (3) In terms of correlation, from 2004–2019, the correlation coefficients of NTL and LST and the bivariate Moran's I within the sixth ring road of Beijing are positive and significant. This shows that there is a significant positive correlation and spatial positive correlation between them. From 2004 to 2009, the temperature increase caused by urbanization was suppressed due to the 2008 Beijing Olympics and related ecological protection policies, resulting in a significant decrease in the correlation coefficient between NTL and LST. From 2009 to 2019, some short-term measures taken by Beijing during the Olympic Games were no longer effective, and the opposition between urban development and related policies made the policies increasingly less effective. The efficient ecological policies in the early period were unable to suppress the LST increase triggered by rapid urbanization in the later period, leading to the correlation coefficient between NTL and LST continued to increase, and the correlation coefficient value in 2019 was higher than that in 2004. The increase in the LST was more significant, which will greatly affect the urban ecological environment and residents' health, making the previous government investment to suppress the temperature increase all in vain.

Therefore, when governments formulate plans for cities at different stages of urbanization, they should enact corresponding strict green policies that can be adhered to in the long term to control the rapidly rising temperatures. This study can provide theoretical and practical support for the development of thermal environment optimization schemes and LST mitigation strategies in Beijing and other cities.

Author Contributions: Conceptualization, Z.L. and F.W.; methodology, F.W.; software, Z.L.; validation, S.W. and H.M.; formal analysis, Z.L.; data curation, Z.L., H.M. and Z.X.; writing—original draft preparation, Z.L.; writing—review and editing F.W., H.M. and Z.X.; funding acquisition, S.W. All authors have read and agreed to the published version of the manuscript.

Funding: This research study was supported by Basic Research Program of Shanxi Province (grant no. 20210302123403), Philosophy and Social Sciences Planning Project of Shanxi Province (grant no. 2020YJ052), Shanxi Provincial People's Government Major Decision Consulting Project (grant no. ZB20211703), the National Natural Science Foundation of China (grant no. 41971233, 41771178, 42030409), the Fundamental Research Funds for the Central Universities (grant no. N2111003), Basic Scientific Research Project (Key Project) of the Education Department of Liaoning Province (grant no. LJKZ0964), Natural Science Foundation of Guizhou Province (grant no. [2019]1150), and the Second Tibetan Plateau Scientific Expedition and Research Program (STEP) (grant no. 2019QZKK1004).

Data Availability Statement: The data presented in this study are available on request from the corresponding author.

Acknowledgments: We greatly thank the reviewers and editors for their constructive suggestions and comments. The authors would like to acknowledge all colleagues and friends who have voluntarily reviewed the translation of the survey and the manuscript of this study.

Conflicts of Interest: The authors declare no conflict of interest.

References

- Kuang, W.; Chi, W.; Lu, D.; Dou, Y. A Comparative Analysis of Megacity Expansions in China and the U.S.: Patterns, Rates and Driving Forces. *Landsc. Urban Plan.* **2014**, *132*, 121–135. [[CrossRef](#)]
- Luo, X.; Yang, J.; Sun, W.; He, B. Suitability of Human Settlements in Mountainous Areas from the Perspective of Ventilation: A Case Study of the Main Urban Area of Chongqing. *J. Clean. Prod.* **2021**, *310*, 127467. [[CrossRef](#)]
- Lai, L.W.; Cheng, W.L. Air Quality Influenced by Urban Heat Island Coupled with Synoptic Weather Patterns. *Sci. Total Environ.* **2009**, *407*, 2724–2733. [[CrossRef](#)] [[PubMed](#)]
- Zhao, C.; Jensen, J.L.R.; Weng, Q.; Currit, N.; Weaver, R. Use of Local Climate Zones to Investigate Surface Urban Heat Islands in Texas. *GIScience Remote Sens.* **2020**, *57*, 1083–1101. [[CrossRef](#)]
- Liu, Y.; Li, Q.; Yang, L.; Mu, K.; Liu, J. Urban Heat Island Effects of Various Urban Morphologies under Regional Climate Conditions. *Sci. Total Environ.* **2020**, *743*, 140589. [[CrossRef](#)]
- Zhao, Z.; Sharifi, A.; Dong, X.; Shen, L.; He, B.-J. Spatial Variability and Temporal Heterogeneity of Surface Urban Heat Island Patterns and the Suitability of Local Climate Zones for Land Surface Temperature Characterization. *Remote Sens.* **2021**, *13*, 4338. [[CrossRef](#)]
- Yang, X.; Peng, L.L.H.; Jiang, Z.; Chen, Y.; Yao, L.; He, Y.; Xu, T. Impact of Urban Heat Island on Energy Demand in Buildings: Local Climate Zones in Nanjing. *Appl. Energy* **2020**, *260*, 114279. [[CrossRef](#)]
- Ren, J.; Yang, J.; Zhang, Y.; Xiao, X.; Xia, J.C.; Li, X.; Wang, S. Exploring Thermal Comfort of Urban Buildings Based on Local Climate Zones. *J. Clean. Prod.* **2022**, *340*, 130744. [[CrossRef](#)]
- Chen, Y.; Yang, J.; Yang, R.; Xiao, X.; Xia, J. Contribution of Urban Functional Zones to the Spatial Distribution of Urban Thermal Environment. *Build. Environ.* **2022**, *216*, 109000. [[CrossRef](#)]
- Liu, M.; Zhang, D.; Pietzarka, U.; Roloff, A. Assessing the Adaptability of Urban Tree Species to Climate Change Impacts: A Case Study in Shanghai. *Urban For. Urban Green.* **2021**, *62*, 127186. [[CrossRef](#)]
- Nasrollahi, N.; Ghosouri, A.; Khodakarami, J.; Taleghani, M. Heat-Mitigation Strategies to Improve Pedestrian Thermal Comfort in Urban Environments: A Review. *Sustainability* **2020**, *12*, 10000. [[CrossRef](#)]
- Yang, J.; Wang, Y.; Xiu, C.; Xiao, X.; Jin, C. Optimizing Local Climate Zones to Mitigate Urban Heat Island Effect in Human Settlements. *J. Clean. Prod.* **2020**, *275*, 123767. [[CrossRef](#)]
- Biardeau, L.T.; Davis, L.W.; Gertler, P.; Wolfram, C. Heat Exposure and Global Air Conditioning. *Nat Sustain.* **2020**, *3*, 25–28. [[CrossRef](#)]
- Yu, H.; Yang, J.; Li, T.; Jin, Y.; Sun, D. Morphological and Functional Polycentric Structure Assessment of Megacity: An Integrated Approach with Spatial Distribution and Interaction. *Sustain. Cities Soc.* **2022**, *80*, 103800. [[CrossRef](#)]
- Imhoff, M.L.; Zhang, P.; Wolfe, R.E.; Bounoua, L. Remote Sensing of the Urban Heat Island Effect across Biomes in the Continental USA. *Remote Sens. Environ.* **2010**, *114*, 504–513. [[CrossRef](#)]
- Estoque, R.C.; Murayama, Y.; Myint, S.W. Effects of Landscape Composition and Pattern on Land Surface Temperature: An Urban Heat Island Study in the Megacities of Southeast Asia. *Sci. Total Environ.* **2017**, *577*, 349–359. [[CrossRef](#)]
- Yao, R.; Wang, L.; Huang, X.; Niu, Z.; Liu, F.; Wang, Q. Temporal Trends of Surface Urban Heat Islands and Associated Determinants in Major Chinese Cities. *Sci. Total Environ.* **2017**, *609*, 742–754. [[CrossRef](#)]
- Yang, J.; Yang, Y.; Sun, D.; Jin, C.; Xiao, X. Influence of Urban Morphological Characteristics on Thermal Environment. *Sustain. Cities Soc.* **2021**, *72*, 103045. [[CrossRef](#)]
- Sultana, S.; Satyanarayana, A.N.V. Assessment of Urbanisation and Urban Heat Island Intensities Using Landsat Imageries during 2000–2018 over a Sub-Tropical Indian City. *Sustain. Cities Soc.* **2020**, *52*, 101846. [[CrossRef](#)]
- El Kenawy, A.M.; Hereher, M.; Robaa, S.M.; McCabe, M.F.; Lopez-Moreno, J.I.; Domínguez-Castro, F.; Gaber, I.M.; Al-Awadhi, T.; Al-Buloshi, A.; Al Nasiri, N.; et al. Nocturnal Surface Urban Heat Island over Greater Cairo: Spatial Morphology, Temporal Trends and Links to Land-Atmosphere Influences. *Remote Sens.* **2020**, *12*, 3889. [[CrossRef](#)]
- Mohammad, P.; Goswami, A.; Bonafoni, S. The Impact of the Land Cover Dynamics on Surface Urban Heat Island Variations in Semi-Arid Cities: A Case Study in Ahmedabad City, India, Using Multi-Sensor/Source Data. *Sensors* **2019**, *19*, 3701. [[CrossRef](#)] [[PubMed](#)]
- Haashemi, S.; Weng, Q.; Darvishi, A.; Alavipanah, S. Seasonal Variations of the Surface Urban Heat Island in a Semi-Arid City. *Remote Sens.* **2016**, *8*, 352. [[CrossRef](#)]
- Yang, J.; Wang, Y.; Xiao, X.; Jin, C.; Xia, J.; Li, X. Spatial Differentiation of Urban Wind and Thermal Environment in Different Grid Sizes. *Urban Clim.* **2019**, *28*, 100458. [[CrossRef](#)]
- Liu, W.; Meng, Q.; Allam, M.; Zhang, L.; Hu, D.; Menenti, M. Driving Factors of Land Surface Temperature in Urban Agglomerations: A Case Study in the Pearl River Delta, China. *Remote Sens.* **2021**, *13*, 2858. [[CrossRef](#)]
- Chen, X.-L.; Zhao, H.-M.; Li, P.-X.; Yin, Z.-Y. Remote Sensing Image-Based Analysis of the Relationship between Urban Heat Island and Land Use/Cover Changes. *Remote Sens. Environ.* **2006**, *104*, 133–146. [[CrossRef](#)]
- Tariq, A.; Shu, H.; Siddiqui, S.; Imran, M.; Farhan, M. Monitoring Land Use And Land Cover Changes Using Geospatial Techniques, A Case Study Of Fateh Jang, Attock, Pakistan. *GES* **2021**, *14*, 41–52. [[CrossRef](#)]
- Tariq, A.; Shu, H. CA-Markov Chain Analysis of Seasonal Land Surface Temperature and Land Use Land Cover Change Using Optical Multi-Temporal Satellite Data of Faisalabad, Pakistan. *Remote Sens.* **2020**, *12*, 3402. [[CrossRef](#)]

28. Yao, L.; Li, T.; Xu, M.; Xu, Y. How the Landscape Features of Urban Green Space Impact Seasonal Land Surface Temperatures at a City-Block-Scale: An Urban Heat Island Study in Beijing, China. *Urban For. Urban Green.* **2020**, *52*, 126704. [[CrossRef](#)]
29. Singh, P.; Kikon, N.; Verma, P. Impact of Land Use Change and Urbanization on Urban Heat Island in Lucknow City, Central India. A Remote Sensing Based Estimate. *Sustain. Cities Soc.* **2017**, *32*, 100–114. [[CrossRef](#)]
30. Majeed, M.; Tariq, A.; Anwar, M.M.; Khan, A.M.; Arshad, F.; Mumtaz, F.; Farhan, M.; Zhang, L.; Zafar, A.; Aziz, M.; et al. Monitoring of Land Use–Land Cover Change and Potential Causal Factors of Climate Change in Jhelum District, Punjab, Pakistan, through GIS and Multi-Temporal Satellite Data. *Land* **2021**, *10*, 1026. [[CrossRef](#)]
31. Dai, Z.; Guldmann, J.-M.; Hu, Y. Spatial Regression Models of Park and Land-Use Impacts on the Urban Heat Island in Central Beijing. *Sci. Total Environ.* **2018**, *626*, 1136–1147. [[CrossRef](#)] [[PubMed](#)]
32. Morabito, M.; Crisci, A.; Guerri, G.; Messeri, A.; Congedo, L.; Munafò, M. Surface Urban Heat Islands in Italian Metropolitan Cities: Tree Cover and Impervious Surface Influences. *Sci. Total Environ.* **2021**, *751*, 142334. [[CrossRef](#)] [[PubMed](#)]
33. Meng, Q.; Zhang, L.; Sun, Z.; Meng, F.; Wang, L.; Sun, Y. Characterizing Spatial and Temporal Trends of Surface Urban Heat Island Effect in an Urban Main Built-up Area: A 12-Year Case Study in Beijing, China. *Remote Sens. Environ.* **2018**, *204*, 826–837. [[CrossRef](#)]
34. Yuan, F.; Bauer, M.E. Comparison of Impervious Surface Area and Normalized Difference Vegetation Index as Indicators of Surface Urban Heat Island Effects in Landsat Imagery. *Remote Sens. Environ.* **2007**, *106*, 375–386. [[CrossRef](#)]
35. Li, Y.; Sun, Y.; Li, J.; Gao, C. Socioeconomic Drivers of Urban Heat Island Effect: Empirical Evidence from Major Chinese Cities. *Sustain. Cities Soc.* **2020**, *63*, 102425. [[CrossRef](#)]
36. Peng, J.; Jia, J.; Liu, Y.; Li, H.; Wu, J. Seasonal Contrast of the Dominant Factors for Spatial Distribution of Land Surface Temperature in Urban Areas. *Remote Sens. Environ.* **2018**, *215*, 255–267. [[CrossRef](#)]
37. Dewan, A.; Kiselev, G.; Botje, D.; Mahmud, G.I.; Bhuiyan, M.H.; Hassan, Q.K. Surface Urban Heat Island Intensity in Five Major Cities of Bangladesh: Patterns, Drivers and Trends. *Sustain. Cities Soc.* **2021**, *71*, 102926. [[CrossRef](#)]
38. Portela, C.I.; Massi, K.G.; Rodrigues, T.; Alcântara, E. Impact of Urban and Industrial Features on Land Surface Temperature: Evidences from Satellite Thermal Indices. *Sustain. Cities Soc.* **2020**, *56*, 102100. [[CrossRef](#)]
39. Zhou, W.; Huang, G.; Cadenasso, M.L. Does Spatial Configuration Matter? Understanding the Effects of Land Cover Pattern on Land Surface Temperature in Urban Landscapes. *Landsc. Urban Plan.* **2011**, *102*, 54–63. [[CrossRef](#)]
40. Maimaitiyiming, M.; Ghulam, A.; Tiyyip, T.; Pla, F.; Latorre-Carmona, P.; Halik, Ü.; Sawut, M.; Caetano, M. Effects of Green Space Spatial Pattern on Land Surface Temperature: Implications for Sustainable Urban Planning and Climate Change Adaptation. *ISPRS J. Photogramm. Remote Sens.* **2014**, *89*, 59–66. [[CrossRef](#)]
41. Tariq, A.; Riaz, I.; Ahmad, Z.; Yang, B.; Amin, M.; Kausar, R.; Andleeb, S.; Farooqi, M.A.; Rafiq, M. Land Surface Temperature Relation with Normalized Satellite Indices for the Estimation of Spatio-Temporal Trends in Temperature among Various Land Use Land Cover Classes of an Arid Potohar Region Using Landsat Data. *Env. Earth Sci* **2020**, *79*, 40. [[CrossRef](#)]
42. Du, Z.W.; Li, X. Growth or shrinkage: New phenomena of regional development in the rapidly-urbanising Pearl River Delta. *Acta Geogr. Sin.* **2017**, *72*, 1800–1811. [[CrossRef](#)]
43. Elvidge, C.D.; Baugh, K.E.; Kihn, E.A.; Kroehl, H.W.; Davis, E.R. Mapping City Lights with Nighttime Data from the DMSP Operational Linescan System. *Eng Remote Sens* **1997**, *63*, 727–734. [[CrossRef](#)]
44. Sutton, P.C. A Scale-Adjusted Measure of “Urban Sprawl” Using Nighttime Satellite Imagery. *Remote Sens. Environ.* **2003**, *86*, 353–369. [[CrossRef](#)]
45. Sutton, P.; Roberts, D.; Elvidge, C.; Melj, H. A Comparison of Nighttime Satellite Imagery and Population Density for the Continental United States. *Photogramm. Eng. Remote Sens.* **1997**, *63*, 1303–1313. [[CrossRef](#)]
46. Sutton, P.C.; Costanza, R. Global Estimates of Market and Non-Market Values Derived from Nighttime Satellite Imagery, Land Cover, and Ecosystem Service Valuation. *Ecol. Econ.* **2002**, *41*, 509–527. [[CrossRef](#)]
47. He, C.; Ma, Q.; Liu, Z.; Zhang, Q. Modeling the Spatiotemporal Dynamics of Electric Power Consumption in Mainland China Using Saturation-Corrected DMSP/OLS Nighttime Stable Light Data. *Int. J. Digit. Earth* **2014**, *7*, 993–1014. [[CrossRef](#)]
48. Doll, C.H.; Muller, J.P.; Elvidge, C.D. Night-Time Imagery as a Tool for Global Mapping of Socioeconomic Parameters and Greenhouse Gas Emissions. *Ambio A J. Hum. Environ.* **2000**, *29*, 157–162. [[CrossRef](#)]
49. Li, J.; Wang, F.; Fu, Y.; Guo, B.; Zhao, Y.; Yu, H. A Novel SUHI Referenced Estimation Method for Multicenters Urban Agglomeration Using DMSP/OLS Nighttime Light Data. *IEEE J. Sel. Top. Appl. Earth Obs. Remote Sens.* **2020**, *13*, 1416–1425. [[CrossRef](#)]
50. Stathakis, D.; Baltas, P. Seasonal Population Estimates Based on Night-Time Lights. *Comput. Environ. Urban Syst.* **2018**, *68*, 133–141. [[CrossRef](#)]
51. Ma, T.; Zhou, Y.K.; Zhou, C.H. Night-Time Light Derived Estimation of Spatio-Temporal Characteristics of Urbanization Dynamics Using DMSP/OLS Satellite Data. *Remote Sens. Environ.* **2015**, *158*, 453–464. [[CrossRef](#)]
52. Sun, Y.; Wang, S.; Zhang, X.; Chan, T.O.; Wu, W. Estimating Local-Scale Domestic Electricity Energy Consumption Using Demographic, Nighttime Light Imagery and Twitter Data. *Energy* **2021**, 120–351. [[CrossRef](#)]
53. Huang, X.; Wang, Y. Investigating the Effects of 3D Urban Morphology on the Surface Urban Heat Island Effect in Urban Functional Zones by Using High-Resolution Remote Sensing Data: A Case Study of Wuhan, Central China. *ISPRS J. Photogramm. Remote Sens.* **2019**, *152*, 119–131. [[CrossRef](#)]

54. Li, W.; Han, C.; Li, W.; Zhou, W.; Han, L. Multi-Scale Effects of Urban Agglomeration on Thermal Environment: A Case of the Yangtze River Delta Megaregion, China. *Sci. Total Environ.* **2020**, *713*, 136556. [[CrossRef](#)] [[PubMed](#)]
55. Zhou, D.; Bonafoni, S.; Zhang, L.; Wang, R. Remote Sensing of the Urban Heat Island Effect in a Highly Populated Urban Agglomeration Area in East China. *Sci. Total Environ.* **2018**, *628–629*, 415–429. [[CrossRef](#)] [[PubMed](#)]
56. Yang, C.; Zhan, Q.; Gao, S.; Liu, H. How Do the Multi-Temporal Centroid Trajectories of Urban Heat Island Correspond to Impervious Surface Changes: A Case Study in Wuhan, China. *Int. J. Environ. Res. Public Health* **2019**, *16*, 3865. [[CrossRef](#)]
57. Yang, Z.W.; Chen, Y.B.; Qian, Q.L.; Wu, Z.F.; Zheng, Z.H.; Huang, Q.Y. The Coupling Relationship between Construction Land Expansion and High-Temperature Area Expansion in China's Three Major Urban Agglomerations. *Int. J. Remote Sens.* **2019**, *40*, 6680–6699. [[CrossRef](#)]
58. Liu, N.; Liu, C.; Xia, Y.; Da, B. Examining the Coordination between Urbanization and Eco-Environment Using Coupling and Spatial Analyses: A Case Study in China. *Ecol. Indic.* **2018**, *93*, 1163–1175. [[CrossRef](#)]
59. Lefever, D.W. Measuring Geographic Concentration by Means of the Standard Deviation Ellipse. *Am. J. Sociol.* **1926**, *32*, 88–94. [[CrossRef](#)]
60. Zhao, Y.; Luo, Z.J.; Li, Y.T.; Guo, J.Y.; Lai, X.H.; Song, J. Study of the spatial-temporal variation of landscape ecological risk in the upper reaches of the Ganjiang River Basin based on the "production-living-ecological space". *Acta Ecol. Sin.* **2019**, *39*, 4676–4686. [[CrossRef](#)]
61. He, B.-J.; Wang, J.; Zhu, J.; Qi, J. Beating the Urban Heat: Situation, Background, Impacts and the Way Forward in China. *Renew. Sustain. Energy Rev.* **2022**, *161*, 112350. [[CrossRef](#)]
62. Piantek, M.; Miguel, J.; Kruger, A.; NaviO, C.; Bernien, M.; Ball, D.K.; Hermann, K.; Kuch, W. Temperature, Surface, and Coverage-Induced Conformational Changes of Azobenzene Derivatives on Cu(001). *J. Phys. Chem. C* **2009**, *113*, 20307–20315. [[CrossRef](#)]
63. Xiong, Y.; Zhang, F. Effect of Human Settlements on Urban Thermal Environment and Factor Analysis Based on Multi-Source Data: A Case Study of Changsha City. *J. Geogr. Sci.* **2021**, *31*, 819–838. [[CrossRef](#)]
64. Shen, Z.J.; Zeng, J. Spatial relationship of urban development to land surface temperature in three cities of southern Fujian. *Acta Geogr. Sin.* **2021**, *76*, 566–583. [[CrossRef](#)]
65. Yao, L.; Xu, Y.; Zhang, B. Effect of Urban Function and Landscape Structure on the Urban Heat Island Phenomenon in Beijing, China. *Landsc. Ecol. Eng.* **2019**, *15*, 379–390. [[CrossRef](#)]
66. Yu, Z.; Yao, Y.; Yang, G.; Wang, X.; Vejre, H. Spatiotemporal Patterns and Characteristics of Remotely Sensed Region Heat Islands during the Rapid Urbanization (1995–2015) of Southern China. *Sci. Total Environ.* **2019**, *674*, 242–254. [[CrossRef](#)]
67. Min, M.; Lin, C.; Duan, X.; Jin, Z.; Zhang, L. Spatial Distribution and Driving Force Analysis of Urban Heat Island Effect Based on Raster Data: A Case Study of the Nanjing Metropolitan Area, China. *Sustain. Cities Soc.* **2019**, *50*, 101637. [[CrossRef](#)]
68. Liu, G.; Zhang, Q.; Li, G.; Doronzo, D.M. Response of Land Cover Types to Land Surface Temperature Derived from Landsat-5 TM in Nanjing Metropolitan Region, China. *Env. Earth Sci.* **2016**, *75*, 1386. [[CrossRef](#)]
69. Yue, W.; Qiu, S.; Xu, H.; Xu, L.; Zhang, L. Polycentric Urban Development and Urban Thermal Environment: A Case of Hangzhou, China. *Landsc. Urban Plan.* **2019**, *189*, 58–70. [[CrossRef](#)]
70. Chen, S.; Hu, D.; Wong, M.S.; Ren, H.; Cao, S.; Yu, C.; Ho, H.C. Characterizing Spatiotemporal Dynamics of Anthropogenic Heat Fluxes: A 20-Year Case Study in Beijing–Tianjin–Hebei Region in China. *Environ. Pollut.* **2019**, *249*, 923–931. [[CrossRef](#)]
71. Zhao, Z.Q. Global Statistics of Spatial Distribution: A Literature Review. *Prog. Geogr.* **2009**, *28*, 1–8. [[CrossRef](#)]
72. Yang, Y.; Ma, M.; Zhu, X.; Ge, W. Research on Spatial Characteristics of Metropolitan Development Using Nighttime Light Data: NTL Based Spatial Characteristics of Beijing. *PLoS ONE* **2020**, *15*, e0242663. [[CrossRef](#)] [[PubMed](#)]
73. Sun, Y.; Wang, S.; Wang, Y. Estimating Local-Scale Urban Heat Island Intensity Using Nighttime Light Satellite Imagery. *Sustain. Cities Soc.* **2020**, *57*, 102125. [[CrossRef](#)]
74. Chen, W.; Zhang, Y.; Pengwang, C.; Gao, W. Evaluation of Urbanization Dynamics and Its Impacts on Surface Heat Islands: A Case Study of Beijing, China. *Remote Sens.* **2017**, *9*, 453. [[CrossRef](#)]
75. Chen, W.; Zhang, Y.; Gao, W.; Zhou, D. The Investigation of Urbanization and Urban Heat Island in Beijing Based on Remote Sensing. *Procedia—Soc. Behav. Sci.* **2016**, *216*, 141–150. [[CrossRef](#)]
76. Dong, X.; Meng, Z.; Wang, Y.; Zhang, Y.; Sun, H.; Wang, Q. Monitoring Spatiotemporal Changes of Impervious Surfaces in Beijing City Using Random Forest Algorithm and Textural Features. *Remote Sens.* **2021**, *13*, 153. [[CrossRef](#)]
77. Xie, P.; Yang, J.; Sun, W.; Xiao, X.; Cecilia Xia, J. Urban Scale Ventilation Analysis Based on Neighborhood Normalized Current Model. *Sustain. Cities Soc.* **2022**, *80*, 103746. [[CrossRef](#)]
78. Ye, H.; Li, Z.; Zhang, N.; Leng, X.; Meng, D.; Zheng, J.; Li, Y. Variations in the Effects of Landscape Patterns on the Urban Thermal Environment during Rapid Urbanization (1990–2020) in Megacities. *Remote Sens.* **2021**, *13*, 3415. [[CrossRef](#)]
79. Chen, L.; Wang, X.; Cai, X.; Yang, C.; Lu, X. Combined Effects of Artificial Surface and Urban Blue-Green Space on Land Surface Temperature in 28 Major Cities in China. *Remote Sens.* **2022**, *14*, 448. [[CrossRef](#)]
80. Kyriakodis, G.-E.; Santamouris, M. Using Reflective Pavements to Mitigate Urban Heat Island in Warm Climates—Results from a Large Scale Urban Mitigation Project. *Urban Clim.* **2018**, *24*, 326–339. [[CrossRef](#)]
81. Middel, A.; Turner, V.K.; Schneider, F.A.; Zhang, Y.; Stiller, M. Solar Reflective Pavements—A Policy Panacea to Heat Mitigation? *Environ. Res. Lett.* **2020**, *15*, 064016. [[CrossRef](#)]

82. Kousis, I.; Fabiani, C.; Gobbi, L.; Pisello, A.L. Phosphorescent-Based Pavements for Counteracting Urban Overheating—A Proof of Concept. *Sol. Energy* **2020**, *202*, 540–552. [[CrossRef](#)]
83. Susca, T.; Gaffin, S.R.; Dell’Osso, G.R. Positive Effects of Vegetation: Urban Heat Island and Green Roofs. *Environ. Pollut.* **2011**, *159*, 2119–2126. [[CrossRef](#)] [[PubMed](#)]
84. Dong, J.; Lin, M.; Zuo, J.; Lin, T.; Liu, J.; Sun, C.; Luo, J. Quantitative Study on the Cooling Effect of Green Roofs in a High-Density Urban Area—A Case Study of Xiamen, China. *J. Clean. Prod.* **2020**, *255*, 120152. [[CrossRef](#)]
85. Doulos, L.; Santamouris, M.; Livada, I. Passive Cooling of Outdoor Urban Spaces. The Role of Materials. *Sol. Energy* **2004**, *77*, 231–249. [[CrossRef](#)]
86. Lei, J.; Kumarasamy, K.; Zingre, K.T.; Yang, J.; Wan, M.P.; Yang, E.-H. Cool Colored Coating and Phase Change Materials as Complementary Cooling Strategies for Building Cooling Load Reduction in Tropics. *Appl. Energy* **2017**, *190*, 57–63. [[CrossRef](#)]
87. Yang, L.; Yu, K.; Ai, J.; Liu, Y.; Yang, W.; Liu, J. Dominant Factors and Spatial Heterogeneity of Land Surface Temperatures in Urban Areas: A Case Study in Fuzhou, China. *Remote Sens.* **2022**, *14*, 1266. [[CrossRef](#)]
88. Azhdari, A.; Soltani, A.; Alidadi, M. Urban Morphology and Landscape Structure Effect on Land Surface Temperature: Evidence from Shiraz, a Semi-Arid City. *Sustain. Cities Soc.* **2018**, *41*, 853–864. [[CrossRef](#)]
89. Chen, M.; Dai, F.; Yang, B.; Zhu, S. Effects of Neighborhood Green Space on PM_{2.5} Mitigation: Evidence from Five Megacities in China. *Build. Environ.* **2019**, *156*, 33–45. [[CrossRef](#)]
90. Yao, X.; Yu, K.; Zeng, X.; Lin, Y.; Ye, B.; Shen, X.; Liu, J. How Can Urban Parks Be Planned to Mitigate Urban Heat Island Effect in “Furnace Cities”? An Accumulation Perspective. *J. Clean. Prod.* **2022**, *330*, 129852. [[CrossRef](#)]
91. Marković, M.; Cheema, J.; Teofilović, A.; Čepić, S.; Popović, Z.; Tomićević-Dubljević, J.; Pause, M. Monitoring of Spatiotemporal Change of Green Spaces in Relation to the Land Surface Temperature: A Case Study of Belgrade, Serbia. *Remote Sens.* **2021**, *13*, 3846. [[CrossRef](#)]
92. Amir Siddique, M.; Wang, Y.; Xu, N.; Ullah, N.; Zeng, P. The Spatiotemporal Implications of Urbanization for Urban Heat Islands in Beijing: A Predictive Approach Based on CA–Markov Modeling (2004–2050). *Remote Sens.* **2021**, *13*, 4697. [[CrossRef](#)]
93. Yang, Y.M.; Park, J.H.; An, S.I.; Wang, B.; Luo, X. Mean Sea Surface Temperature Changes Influence ENSO-Related Precipitation Changes in the Mid-Latitudes. *Nat. Commun.* **2021**, *12*, 1495. [[CrossRef](#)] [[PubMed](#)]